Accepted manuscript doi:
10.1680/jmacr.18.00156

Accepted manuscript doi:
10.1680/jmacr.18.00156

Submitted: 26 March 2018

Published online in 'accepted manuscript' format: 28 August 2018

Manuscript title: A numerical investigation of the cracking behaviour of reinforced concrete tie elements

Authors: Reignard Tan[1], Max A. N. Hendriks[1,2], Mette Geiker[1] and Terje Kanstad[1]

Affiliations: [1]Department of Structural Engineering, Norwegian University of Science and Technology, Trondheim, Norway and [2]Faculty of Civil Engineering & Geosciences, Delft University of Technology, Delft, The Netherlands

Corresponding author: Reignard Tan, Multiconsult AS, Postboks 265 Skøyen, 0213 Oslo, Norway. Tel.: +4741561203.

E-mail: reignard.tan@multiconsult.no

Accepted manuscript doi:
10.1680/jmacr.18.00156

Abstract

The cracking behaviour of reinforced concrete (RC) ties are investigated by conducting virtual experiments using nonlinear finite element analysis (NLFEA). The assumptions in the model are verified by benchmarking the classical experiments of Bresler and Bertero (1968) and Yannopoulos (1989), which shows good agreement in comparison of steel strains, development of crack widths and crack spacing. Furthermore, virtual experiments on four difference RC ties show that the size of the cover and not the bar diameter governs the crack spacing and thus implicitly the crack width. An increase of the bar diameter has a beneficial effect in reducing the steel stress and the associated steel strains, which in turn reduces the crack width. Finally, a single bond-slip curve is sufficient in describing the average bond transfer of an arbitrary RC tie.

Keywords: Cracks & cracking; bond; finite element methods

Accepted manuscript doi:
10.1680/jmacr.18.00156

1. Introduction

In deriving an analytical crack width calculation model for reinforced concrete (RC) elements, the role of (i) bond at the steel-concrete interface and (ii) cover becomes two key parameters (CEB, 1985; Balász et al., 2013). This paper investigates these two parameters using nonlinear finite element analyses (NLFEA), which were validated against classical experiments. The tensile strength of concrete, is a third key parameter. This parameter has been investigated thoroughly in the research project of CEOS.fr (2016) at which the scale effect is accounted for in determining the concrete tensile strength, and will not be addressed in detail here.

The role of bond and cover are implemented in the *empirical* formulation recommended by ACI (ACI, 2001), and in the *semi-empirical* formulation recommended by Eurocode 2 (EC2) (CEN, 2004) and *fib* Model Code 2010 (MC2010) (*fib*, 2013) in a relatively simplified manner. The bond and cover term in the crack spacing formula of EC2 and MC2010 are based on two different mechanical models and are as such in conflict with the basic principles in statics (Tan et al., 2018a). The authors in this paper claim that a more mechanically consistent crack width calculation model can be formulated by including the two key parameters in deriving and solving the second order differential equation for the slip. In such an analytical model, the choice of a local bond-slip curve becomes essential. While the relevance of a local bond-slip curve is well understood for pull-out tests (*fib*, 2000), this seems not to be the case for RC ties subjected to pure tension. Although several authors have contributed in the discussions by conducting experiments on concentric tension specimens (Nilson, 1972; Dörr, 1978; Mirza and Houde, 1979; Somayaji and Shah, 1981; Jiang et al., 1984), the answer to the question of what a local bond-slip model physically represents in an RC tie subjected to pure tension still remains unclear. There seems to be consensus in the literature (Russo and Romano, 1992; Balász, 1993; Debernardi and Taliano, 2013; Debernardi and Taliano, 2016) in choosing the local bond-slip model proposed by Eligehausen et al. (1983) and later adopted by MC2010. The parameters involved, however, were determined empirically based on pull-out tests in which the confining concrete is subjected to compression. The problem thus becomes related to choosing proper values that are representative in the case of RC ties subjected to pure tension.

In this study, the authors seek to contribute to a better understanding of the cracking behaviour of RC ties with deformed steel bars subjected to pure tension by conducting virtual experiments using NLFEA. Such virtual experiments offers the possibility of monitoring the internal behaviour of the confining concrete, a convenience

that often is limited in physical experiments. First, important assumptions in the finite element (FE) model are discussed. Secondly, the classical experiments of Bresler and Bertero (1968) and Yannopoulos (1989) are benchmarked to investigate the validity of the assumptions in the FE-model and the cracking behaviour of RC ties. Then, the role of bar diameter and cover are investigated and discussed by conducting virtual experiments on four different RC ties. Finally, values for the parameters in the local bond-slip curve recommended by MC2010 (*fib, 2013*) are proposed. These can be used in an analytical crack width calculation model after having solved the second order differential equation for the slip. The authors in this paper are currently working on such an approach (Tan et al. (2018b).

2. Finite element model

2.1 Main assumptions

Detailed NLFEA of RC ties with small element sizes (< 10 mm) are normally carried out using interface elements between concrete and steel, e.g. as suggested by Lutz (1970) and conducted by Tammo et al. (2009). This can be useful to include for effects such as the wedging action between the bar ribs and the surrounding concrete without physically modelling the geometry of the bar ribs, as well as including for the effect of slip when adhesion breaks down. In this study, interface elements are used to allow for separation but not any slip, meaning that the concrete at the interface is assumed to follow the longitudinal displacement field of steel completely. This further implies that the bond transfer at the interface is mechanically maintained, although the concrete is separated radially from the steel bar. This assumption is based on the experimental behaviour of RC ties reported in the literature, in which there is a general agreement that the crack width at the steel bar surface is significantly smaller than that on the concrete surface in the case of deformed steel bars (Watstein and Mathey, 1959; Broms, 1968; Husain and Ferguson, 1968; Yannopoulos, 1989; Beeby, 2004; Borosnyói, 2010). The research of Goto (1971) and Tammo and Thelandersson (2009) concludes that this occurs due to the rib interaction between concrete and steel, which causes the concrete to crack internally, thus allowing it to follow the longitudinal displacement field of steel at the interface as depicted in Fig. 1(a).

Note that the assumption of neglecting the crack width at the steel bar surface allows the use of a relatively simple FE-model, in which shear deformations in the steel concrete interface are prohibited and the explicit modelling of the bar ribs is avoided. This means that localized bond stresses that would arise at the bar ribs are

smeared over the rebar. This also implies that effects related to the rib geometry or other bond conditions, e.g. wedging action or slip due to loss of adhesion, cannot be captured in this FE-model. These effects, however, remain normally limited in RC ties with deformed steel bars subjected to pure tension (*fib*, 2000) making the simple FE-model adequate for the purpose of this study.

2.2 Axisymmetric model

The NLFEA were carried out using quadratic, axisymmetric, quadrilateral elements in the finite element program DIANA (DIANA FEA BV, 2016). A linear elastic material model was used for steel, while a non-linear fracture mechanics material model with rotating cracks based on a total strains formulation was used for concrete. The parabolic curve according to Feenstra (1993) was used for the compressive behaviour, while the softening curve according to Hordijk (1991) was used for the tensile behaviour. The Poisson's effect was gradually reduced in accordance with the total strains formulation as the cracking damage progressed, while lateral influences on the compressive behaviour were neglected. Geometry, interface layer, loading and boundary conditions for the FE-model are as shown in Fig. 1(b). Symmetry allowed for modelling half of the length only.

Loads were monotonically increased in a displacement-controlled manner using regular Newton-Raphson iterations. The convergence criteria were force and energy based with the tolerance value of 0.01 and 0.001, respectively, in accordance with the Dutch Guidelines for NLFEA of Concrete Structures (Belletti et al., (2014); Hendriks et al., 2017). The element size was adjusted to obtain approximately 6-10 elements over the cover and 1-3 elements over the steel bar radius.

Interface elements between concrete and steel were chosen to have a thickness of $t_{\mathrm{i}} = 0.1$ mm. A non-linear elasticity model with nonlinear properties in radial direction and a constant stiffness in shear direction were chosen to allow for radial separation only in accordance to the discussed assumptions in the previous section. The elastic radial and shear modulus for the interface elements were derived from the modulus of elasticity for concrete, E_{c}, i.e. respectively as $E_{\mathrm{c}}/t_{\mathrm{i}}$ and $E_{\mathrm{c}}/[2(1+\nu_{\mathrm{c}})t_{\mathrm{i}}]$. The elastic radial modulus was reduced with a factor of 10^{-05} when a tensile strain of $0.8f_{ct}/E_c$ at the interface was reached, in order to simulate the radial separation in a stable manner.

Accepted manuscript doi:
10.1680/jmacr.18.00156

3. Validation of finite element model

3.1 Test set-up

The classical experiments of Bresler and Bertero (1968) and Yannopoulos (1989) were benchmarked to investigate the validity of the assumptions in the FE-model. The investigated RC tie named specimen H by Bresler and Bertero (1968) was 152 mm (6 in) in diameter, had a length of 406 mm (16 in), and was embedded with a deformed steel bar with diameter 28.7 mm (1.13 in) in the centre of the cross-section. The length of the specimen was chosen as twice the mean crack spacing obtained from the pilot studies of 1829 mm (72 in) long RC ties with similar sectional properties. The specimen was axially cyclic loaded in the steel bar ends in the experiments, and a notch was cut at the mid-length to induce a primary crack at this section. Strain gauges were mounted in a sawed-out canal in the centre of the steel bar to measure the steel strains over the length. The reduction of the steel bar area due to the sawed-out canal was accounted for by subtracting an inner radius of 5.6 mm from the outer radius of the steel bar in the FE-model. This corresponded to the given nominal area of 548 mm^2 (0.85 in^2) for the steel bar in the experiments.

The six RC ties investigated by Yannopoulos (1989) were 76 mm in diameter, had a length of 100 mm, and were embedded with a deformed steel bar with diameter 16 mm in the centre of the cross-sections. The length of the specimens was limited to avoid formation of a new primary crack and was based on the mean crack spacing obtained from pilot studies carried out on 800 mm long RC ties with similar sectional properties. The RC ties were axially and monotonically loaded at the steel bar ends while measuring the development of the crack width.

The material parameters given in the experiments are summarized in Table 1 and were used in validating the FE-model. Material parameters such as the Poisson's ratio and the fracture energy were not given in the experiments and were derived in accordance with the recommendations in the Dutch Guidelines for NLFEA of Concrete Structures (Hendriks et al., 2017).

3.2 Comparison of steel strains, crack widths and crack spacing

The comparison of the obtained steel strains from the NLFEA and the experimental steel strains of Bresler and Bertero [(1968)] at four different load levels are shown in Fig. 2(a). The two lowest load levels corresponding to

steel stresses of 33 MPa and 65 MPa give good comparisons of the steel strains, as expected, since the experimental strains at these load levels are obtained from the first monotonic load cycle. The experimental strains at the two higher load levels corresponding to steel stresses of 195 MPa and 242 MPa, however, are obtained from the second load cycle. Cyclic loading is known to have a significant effect on the deterioration of bond even for the first repeated loads (Dörr, 1978; *fib*, 2000), which could explain the less stiff response of the experimental steel strains in the second load cycle compared to that obtained from the monotonic loading in the NLFEA. Nevertheless, the comparison of the steel strains obtained from the NLFEA and the experiments show in general a good agreement.

A comparison of the development of the crack width with increasing steel stresses obtained in the experiments of Yannopoulos (1989) and in the NLFEA is shown in Fig. 2(b). The comparison of the developed crack width also show good agreement, however, it is observed that the NLFEA slightly overestimates the crack width for a given steel stress. .

Separate NLFEA were conducted to investigate if the FE-model also could predict crack spacing similar to that obtained in the pilot studies of Bresler and Bertero (1968) and Yannopoulos (1989) on longer specimens. The RC tie lengths were thus increased in the FE-model to investigate this. The strain distributions in Fig. 3(a) and 3(b) respectively shows that a new crack formed in the NLFEA at a distance of approximately 200 mm from the loaded end for the long "Bresler and Bertero" specimen and at approximately 80 mm for the long "Yannopoulos" specimen. This corresponds well to the mean crack spacing of 203 mm and 90 mm respectively obtained in the experiments of Bresler and Bertero (1968) and Yannopoulos (1989) on longer specimens.

The good agreement in comparison of steel strains, crack widths and crack spacing confirms the validity of the discussed assumptions, and further show the ability of the FE-model to simulate the physical behaviour of RC ties realistically.

Accepted manuscript doi:
10.1680/jmacr.18.00156

4. The physical behaviour of RC ties

4.1 General

The physical behaviour of RC ties is now discussed and elucidated using the results from the NLFEA conducted on the "Bresler and Bertero" specimen. Details for the test set-up were presented in section 3.1. A contour plot of exaggerated radial displacements at a steel stress $\sigma_s \approx 180$ MPa, which is just before a primary crack forms at the symmetry section, is shown in Fig. 4(a). It is noticed that the concrete is separated radially from the steel bar close to the loaded end due to the inflicted shear stress at the concrete inner surface. The radial displacements are counteracted by the stiffness of the concrete in the hoop direction, causing a confining pressure to the steel bar. Splitting cracks arise if the hoop stresses exceed the tensile strength of concrete as can be observed in Fig. 4(b). Actually, the splitting cracks causes a build-up of radial and shear stresses close to the loaded end, before reaching the peaks at the approximately same location over the bar length as can be observed in Fig. 4(c). Further propagation of internal splitting cracks as the load increases causes additional movement of the stress peaks towards the symmetry section.

It should be mentioned that the maximum radial displacements in the analyses are in the magnitude of 10^{-2} mm, which still is small compared to typical rib dimensions. This justifies the assumption of claiming that the mechanical bond is maintained although the concrete is separated radially from the steel bar. Finally, these observations suggests that the shear transfer is dependent on the stiffness of the confining concrete.

4.2 Lightly versus heavily loaded members

The interaction of the load level and the specimen length is significant for the cracking behaviour of RC ties. Russo and Romano (1992) were the first to introduce the principles of the *comparatively lightly loaded member* (CLLM) behaviour and the *comparatively heavily loaded member* (CHLM) behaviour, which are conceptually visualized in Fig. 5(a) and (b) respectively. The figures depict the steel and the corresponding concrete strain distribution of a long specimen with length $L = 500\ mm$ and a short specimen with length $L = 200\ mm$, exposed to the same loading. To clarify, the arrows in Fig. 5(b) indicate the corresponding concrete surface strains to the steel strains for the short specimen. The main difference being is that the strains become compatible ($\varepsilon_s = \varepsilon_c$) at a certain distance x_r from the loaded end and remain constant along the remaining length in the case of CLLM, while in the case of CHLM the strains remain incompatible ($\varepsilon_s > \varepsilon_c$) over the

entire specimen length. The point of compatibility x_r moves towards the symmetry section upon increasing the load, and will have moved completely to the symmetry section ($x_r = L/2$) for a sufficiently large load in the case of CLLM. Upon even further loading, strains become incompatible at the symmetry section and a primary crack will only have the possibility to form here if the concrete strains exceed the cracking strain. The specimen can then be said to have undergone a smooth transition from the CLLM behaviour to the CHLM behaviour. If the concrete strains exceed the cracking strain at any location prior to the symmetry section, i.e. $\varepsilon_c(x_r) \geq \varepsilon_{ct}$, a new primary crack will instead form here thus generating a new member length $L = x_r = x_{cr}$. The new member will then exhibit either a CLLM behaviour or a CHLM behaviour depending on the load level and the member length.

An analogy of the CLLM and CHLM behaviour can be drawn to the so-called *crack formation stage* and *stabilized cracking stage*, respectively. However, they are not the same. This can be explained by the fact that a smooth transition between the CLLM and the CHLM behaviour is possible, which is not the case in the concept of crack formation stage and stabilized cracking stage.

5. The influence of bar diameter and cover on the cracking behaviour of RC ties

5.1 Virtual experiments

The bar diameter and cover are essential parameters in calculating the crack spacing and the crack width in the semi-empirical formulas recommended by EC2 (CEN, 2004) and MC2010 (*fib*, *2013*). Both parameters have been subject of major discussions for several decades in developing the semi-empirical formulas (Saliger, 1936; Base et al., 1966; Ferry-Borges, 1966; Broms, 1968; Gergely and Lutz, 1968; Beeby, 1979; Beeby, 2004; Caldentey et al., 2013; Tan et al., 2018a). For this purpose, the FE-model established and verified in this study has been used to conduct virtual experiments on RC ties to better understand the influence of bar diameter and cover.

The behaviour of four circular specimens, reinforced with one concentric deformed steel bar were investigated. The specimens were named $\phi 20c40$, $\phi 20c90$, $\phi 32c40$ and $\phi 32c90$, indicating that the bar diameter ϕ either was 20 or 32 mm and that the cover c either was 40 mm or 90 mm. A concrete grade C35 according to MC2010

(*fib*, 2013) was chosen for the concrete, while a Young's modulus of $E_s = 200000$ MPa and a yield strength of $f_y = 500$ MPa was chosen for the steel. The Poisson's ratio and the fracture energy were derived in accordance with the recommendations in the Dutch Guidelines for NLFEA of Concrete Structures (Hendriks et al., 2017). The analysis procedure was to first conduct CLLM studies on longer specimens ($L = 700$ mm) to obtain a typical crack spacing x_{cr}, after which a separate analysis on the cracked specimen was conducted to include for the CHLM behaviour.

5.2 The influence of bar diameter

5.2.1 CLLM behaviour

The bond stress distributions for the CLLM behaviour of $\phi 20c40$ vs. $\phi 32c40$ and $\phi 20c90$ vs. $\phi 32c90$ are compared at the load levels just before a primary crack forms in Fig. 6(a) and (b), respectively, with Table 2 showing the corresponding condition in the specimens. The comparison shows that the bond stress distributions are influenced greatly by the bar diameter and differs in general from one another. It is noticed though, that the bond stress distributions align and become negligibly small ($\tau < 1$ MPa) at the approximately same location over the bar length, indicating the end of the *transfer length* and that a primary crack is about to form in the vicinity. The concrete force resultant at a distance s_r from the loaded end is obtained by integrating the bond stress distribution $\tau(x)$ as

$$F_c(x_{cr}) = \int_0^{s_r} \tau(x)\pi\phi dx = \tau_{bm,s_r}\pi\phi x_{cr} \quad (1)$$

which is limited by the cracking force as

$$F_{cr} = f_{ct}A_c \quad (2)$$

Although the bar diameter influences the bond stress distribution and thus the concrete force resultant in Eq. (1), it does not significantly affect the limit value in Eq. (2) nor influence the transfer length as pinpointed out for Fig. 6(a) and (b). This means that a primary crack forms at the approximately same location over the bar length for specimens having similar cover, irrespective of the bar diameter size as also can be observed in Table 2.

5.2.2 CHLM behaviour

The strain distribution for the CHLM behaviour of $\phi 20c40$ vs. $\phi 32c40$ and $\phi 20c90$ vs. $\phi 32c90$ with specimen lengths similar to the crack spacing in Table 2 is shown in Fig. 7(a) and (b) at two steel stress levels, while the development of the crack width with steel stresses is shown in Fig. 7(c) and (d). It is observed that the bar diameter influences the strain distribution over the bar length for a given steel stress. The 20 mm specimens experience more variation in steel strains than the 32 mm specimens. This can be explained by the fact that the 32 mm specimens are exposed to a substantially higher load level than the 20 mm specimens for a given steel stress. This implies that the confining concrete for the 32 mm specimens is exposed to more internal cracking than the 20 mm specimens, which has a significant limiting effect on the tension stiffening. Less tension stiffening results in larger crack width for a given steel stress as can be observed in Fig. 7(c) and (d), which can be explained by the following. The crack width is obtained by integrating the difference in steel strains and concrete strains at the specimen surface over the bar length as

$$w = \int_0^{x_{\mathrm{cr}}} (\varepsilon_{\mathrm{s}} - \varepsilon_{\mathrm{c}}) dx \qquad (3)$$

Acknowledging from Fig. 7(a) and (b) that the concrete strains are negligible in the case of CHLM behaviour, yields that the major contribution to the crack width must be the steel strains. Hence, larger reduction in steel strains over the specimen length results in smaller crack width. It should be mentioned though, that large bar diameters have a beneficial effect in reducing the steel stress and the associated steel strains for a given load level, which in turn reduces the crack width.

5.3 The influence of cover

5.3.1 CLLM behaviour

The bond stress distributions for the CLLM behaviour of $\phi 20c40$ vs. $\phi 20c90$ and $\phi 32c40$ vs. $\phi 32c90$ are compared in Fig. 8(a) and (b), respectively, at two different conditions, one at a similar load level ($\sigma_{\mathrm{s}} \approx 50$ MPa and $\sigma_{\mathrm{s}} \approx 35$ MPa) and the other corresponding to the load levels in Table 2, which is just before a primary crack forms. The comparison of the bond stress distributions at the similar load level shows that they are quite similar, implying that the cover size does not affect the bond transfer significantly for a given load level and bar diameter in the case of CLLM behaviour. However, comparing the bond stress distributions at the load levels

just before a primary crack forms shows that both bond stresses and transfer lengths increase with increasing load level and cover, which can be explained mechanically by the following. A larger cover increases the cracking force in accordance with Eq. (2). The concrete force resultants in accordance with Eq. (1) though, remain approximately the same at the load level just before a primary crack forms in the specimen having a smaller cover since the bond stress distributions should be quite similar for a given load level. This means that the concrete force resultant for the specimen having a larger cover only can increase and approach its cracking force by increasing the load level. This in turn results in a larger bond stress distribution and transfer length, which also can be observed in Table 2 by comparing mean bond stresses and crack spacing for specimens having similar bar diameter but different covers.

5.3.2 CHLM behaviour

The strain distribution for the CHLM behaviour of $\phi 20c40$ vs. $\phi 20c90$ and $\phi 32c40$ vs. $\phi 32c90$ with specimen lengths similar to the crack spacing in Table 2 is shown in Fig. 9(a) and (b), while the development of the crack width with steel stresses is shown in Fig. 9(c) and (d). The specimens $\phi 20c90'$ and $\phi 32c90'$ are included to represent the hypothetical case in which $\phi 20c90$ and $\phi 32c90$ respectively were ought to have the same specimen lengths as $\phi 20c40$ and $\phi 32c40$. It is noticed that the variation in steel strains and the development of crack width nearly remains the same for specimens having similar lengths and bar diameters but different covers. This means that it is the specimen length in which the steel strains are integrated over that governs the crack width and not necessarily the cover itself. Hence, the cover does not explicitly influence the crack width per sé, but contributes implicitly by increasing the crack spacing. Larger crack spacing simply results in larger crack width as indicated in Fig. 9(c) and (d).

5.4 The influence of bar diameter and cover on the crack spacing

The discussions of Fig. 6(a) and (b) and Fig. 8(a) and (b) suggest that the crack spacing is a geometrically dependent parameter, which is mainly governed by the size of the cover but not the bar diameter. Comparable conclusion was drawn by Broms (1968), Gergely and Lutz (1968), Beeby (2004) and Tan et al. (2018a), primarily by discussing the limited influence of ϕ/ρ_{eff} on the development of crack widths observed in several published experiments. A mechanical explanation to this finding is that the concentrated forces inflicted at the steel bar ends at the moment of cracking, $F = \varepsilon_{\text{ct}}(E_{\text{s}}A_{\text{s}} + E_{\text{c}}A_{\text{c}}) \approx f_{\text{ct}}A_{\text{c}}$, should be close for two specimens

Accepted manuscript doi:
10.1680/jmacr.18.00156

having similar cover but different bar diameters since the concrete area A_c remains almost the same as discussed earlier, see Table 2. This means that the concentrated forces inflicted at the steel bar ends should disperse in a similar fashion over the cover to obtain an even distribution of the stresses over the cross section, further implying that the transfer lengths also should be close. Fig. 10(a), which shows how the concrete force resultants gradually increase from the loaded end at the load levels corresponding to Table 2, supports this postulation. Another supporting evidence can be observed in Fig. 10(b), which shows the development of the corresponding concrete surface stresses over the respective transfer lengths.

Although the cover appears to be governing for the crack spacing in virtual experiments, in physical experiments the bar diameter could still have a substantial influence. This is mainly owing to the large scatter of the tensile strength of concrete in real life structures (CEOS.fr, 2016). The influence of the tensile strength will cause a structure to crack more randomly and not necessarily at the end of the transfer length during the crack formation. The division of the member length due to the random cracking will cause an interaction of the CLLM and CHLM behaviour at which both the cover and the bar diameter together play significant roles for the further development of the crack pattern.

Accepted manuscript doi:
10.1680/jmacr.18.00156

6. Local bond-slip curve

6.1 Determining the local bond-slip curves

The slip distributions for the analysed specimens are approximated by numerically integrating the difference in steel and concrete strains over the bar lengths using the method of Riemann sum as

$$s(x) = \int_{x}^{\frac{L}{2}} (\varepsilon_s - \varepsilon_c) dx \approx \sum_{i \mid x \le x_i \le \frac{L}{2}} (\varepsilon_{si} - \varepsilon_{ci})\, \Delta x \tag{4}$$

where

$s(x)$ is the slip at an arbitrary section x

ε_s is strain at the steel surface

ε_c is strain at the outer concrete surface

x_i is the x-coordinate of integration points adjacent to the steel and outer concrete surface

ε_{si} and ε_{ci} are respectively steel and concrete strains at these integrations points

Δx is half the FE length

A 2x2 integration scheme was applied for the FE. Furthermore, using the strains adjacent to the outer concrete surface implies that the slip is composed of two parts: the relative displacement occurring at the interface between concrete and steel due to formation of internally inclined cracks and shear deformations occurring over the cover. This conforms to the definition of slip in accordance with *fib* bulletin No. 10 (2000) and Tan et al. (2018a). Local bond-slip curves are finally obtained by extracting the shear stresses in steel integration points adjacent to the steel bar surface at the location of the evaluated slip.

6.2 The local bond-slip curves

Local bond-slip curves at coordinates $x \approx 0$, $x = L/8$, $x = L/4$, $x = 3L/8$ and $x = L/2$ for steel stresses up to 400 MPa have been extracted from all of the analysed specimens in this study and plotted in Fig. 11. Both CLLM and CHLM behaviour with specimen lengths corresponding to Fig. 6, 7, 8 and 9 have been included in the plots. Fig. 11 shows that the local bond-slip curves in general vary with the geometry of the RC tie. However, there are some significant resemblances. Except for the post peak region, which occurs at relatively large steel stresses, the local bond-slip curves are seen to exhibit quite similar behaviour independent of the

location over the bar length for a given geometry. The exception are the local bond-slip curves located in the vicinity of the primary crack ($x \approx 0$) owing to the combined formation of inclined and splitting cracks taking place here, as could be observed in Fig. 4(b). This suggests that one local bond-slip curve is sufficient in describing the mean bond transfer for a certain RC tie. Moreover, the bond-slip curve includes the effect that the stiffness reduction of the confining concrete has on reducing the bond transfer due to internal cracking.

The local bond-slip curve proposed by Eligehausen et al. [(1983)] and later adopted by MC2010 [(2013)]

$$\tau = \tau_1 \left(\frac{s}{s_1}\right)^{\alpha} \tag{4}$$

is plotted with the parameters $\tau_1 = 5.0$ MPa, $s_1 = 0.1$ mm and $\alpha = 0.35$ in Fig. 11, while Fig. 12 shows all of the obtained bond-slip curves plotted together with Eq. (4). It is seen that the chosen parameters for Eq. (4) tend to serve as a mean for all of the obtained bond-slip curves, irrespective of geometry and location over the bar length. This has an important practical significance in the sense that only one bond-slip curve seems to be necessary in describing the average behaviour of an arbitrary RC tie. In fact, solving the second order differential equation for the slip analytically using the bond slip curve in Eq. (4) is seen to yield both consistent and conservative predictions for the crack width and crack spacing in Tan et al. (2018b). This yields ultimately an analytical model that is capable of replicating the NLFEA conducted in this paper.

7. Conclusions

Based on the findings in this study, the following conclusions can be drawn

- The FE-model used to conduct virtual experiments is based on the assumption that the concrete follows the longitudinal displacement field of steel at the interface, which has proven to predict the cracking behaviour of cylindrical RC ties quite accurately.
- Virtual experiments on four different RC ties show that the crack spacing can be proven mechanically to be a geometrically dependent parameter governed by the size of the cover, and not the bar diameter. In physical experiments, however, the bar diameter could still have a substantial influence. This is due to the large scatter of the tensile strength, which will greatly influence the crack spacing and thus the interaction of the CLLM and CHLM behaviour.
- The cover size does not explicitly increase the crack width per sé, but contributes implicitly by increasing the crack spacing the steel strains are integrated over. Larger crack spacing simply results in larger crack widths.
- Large bar diameters have a beneficial effect in reducing the steel stresses and the appurtenant steel strains, which in turn reduce the crack widths.
- A local bond-slip curve includes for the effect that the stiffness reduction of the confining concrete has on the bond transfer due to internal cracking. Moreover, one bond-slip curve is sufficient in describing the average bond behaviour of an RC tie with arbitrary geometry. This has a practical significance that enables an analytical model capable of replicating the NLFEA results.

Acknowledgements

The work presented in this paper is part of an ongoing PhD study funded by the Norwegian Public Roads Administration as a part of the Coastal Highway Route E39 project.

List of notations

A_c	Area concrete
A_s	Area steel
c	Cover
E_c	Modulus of elasticity concrete
E_s	Modulus of elasticity steel
F_c	Force resultant concrete
F_{cr}	Cracking force concrete
f_c	Compressive strength concrete
f_{ct}	Tensile strength concrete
f_y	Yield strength steel
G_f	Tensile fracture energy concrete
G_{fc}	Compressive fracture energy concrete
L	Bar length
s	Slip
s_1	Slip parameter in bond-slip curve according to MC2010
x	Position over the bar length
x_{cr}	Crack spacing
x_i	x-coordinate of integration points adjacent to the steel and outer concrete surface
x_r	Transfer length
Δx	Half FE length
α	Curve parameter in bond-slip curve according to MC2010
ε_c	Strains at outer concrete surface
ε_{ci}	Concrete strains at integration points
ε_{ct}	Cracking strain concrete
ε_s	Strains at steel surface
ε_{si}	Steel strains at integration points
ν_c	Poisson's ratio concrete
ν_s	Poisson's ratio steel
ρ_{eff}	Reinforcement ratio
σ_s	Steel stress
τ_1	Bond stress parameter in bond-slip curve according to MC2010
$\tau_{bm,x_{cr}}$	Mean bond stress over the crack distance
ϕ	Bar diameter

References

Balázs et al. (2013) Design for SLS according to *fib* Model Code 2010. *fib* Journal Structural Concrete 14(2): 99-123.

Bálasz GL (1993) Cracking Analysis Based on Slip and Bond Stresses. ACI Materials Journal 90(4): 340-348.

Base GD, Read JB, Beeby AW et al. (1966) An investigation of the crack control characteristics of various types of bar in reinforced concrete beams. Research Report 18, Part 1, Cement and Concrete Association, London, UK.

Beeby AW (1979) The prediction of crack widths in hardened concrete. The Structural Engineer 57A(1): 9-17.

Beeby AW (2004) The influence of the parameter ϕ/ρ_{eff} on crack widths. *fib* Journal Structural Concrete 5(2): 71-83.

Belletti B, Damoni C, Hendriks MAN et al. (2014) Analytical and numerical evaluation of the design resistance of reinforced concrete slabs. *fib* Journal Structural Concrete, 15(3): 317-330.

Borosnyói A and Snóbli I (2010) Crack width variation within the concrete cover of reinforced concrete members, Építőanyag – Journal of Silicate Based and Composite Materials 62(3): 70-74.

Bresler B and Bertero VV (1968) Behavior of reinforced concrete under repeated load. Proceedings of the ASCE – Journal of the Structural Division 94(6): 1567-1590.

Broms BB (1968) Theory of the calculation of crack width and crack spacing in reinforced concrete members. Cement och Betong No. 1: 52-64.

Caldentey AP, Peiretti HC, Iribarren JP et al. (2013) Cracking of RC members revisited: influence of cover, $\phi/\rho_{s,ef}$ and stirrup spacing – an experimental and theoretical study. *fib* Journal Structural Concrete, 14(1): 69-78.

CEB (1985) CEB Design Manual on Cracking and Deformations. École Polytechnique Fédérale du Lausanne, Lausanne, Switzerland.

CEN (2004) EN 1992-1-1 Eurocode 2: Design of Concrete Structures – Part 1-1: General Rules and Rules for buildings. European Committee for Standardization, Brussels, Belgium.

CEOS.fr (2016) Control of Cracking in Reinforced Concrete Structures. ISTE Ltd and John Wiley & Sons, Inc, London and Hoboken, UK and USA.

Debernardi PG and Taliano M (2013) Effect of Secondary Cracks for Cracking Analysis of Reinforced Concrete Tie, ACI Materials Journal 110(2): 209-216.

Debernardi PG and Taliano M (2016) An improvement to Eurocode 2 and *fib* Model Code 2010 methods for calculating crack width in RC structures, *fib* Journal Structural Concrete 17(3): 365-376.

DIANA FEA BV (2016) DIANA Finite Element Analysis User's Manual Release 10.1. Delft, The Netherlands.

Dörr K (1978) Bond-Behaviour of Ribbed Reinforcement under Transversal Pressure. IASS Symposium on Nonlinear Behaviour of Reinforced Concrete Spatial Structures, Werner Verlag, Düsseldorf, Germany, Vol. 1, pp. 13-24.

Eligehausen R, Popov EP and Bertero VV (1983) Local bond stress-slip relationships of deformed bars under generalized excitations, Report No. UCB/EERC 83-23, University of California, Berkeley, USA.

Feenstra PH (1993) Computational Aspects of Biaxial Stress in Plain and Reinforced Concrete. PhD thesis, Delft University of Technology, Delft, The Netherlands.

Ferry-Borges J (1966) Cracking and deformability of reinforced concrete beams. IABSE Publications, Vol. 26, pp. 75-95.

fib (2000) Bond of reinforcement in concrete – State-of-art report. *fib* bulletin No. 10, Lausanne, Switzerland.

fib (2013) *fib* Model Code for Concrete Structures 2010. International Federation for Structural Concrete, Ernst & Sohn, Berlin.

Gergely P and Lutz LA (1968) Maximum Crack Width in Reinforced Concrete Flexural Members. Causes, Mechanisms and Control of Cracking in Concrete, SP-20, American Concrete Institute, Farmington Hills, MI, USA, pp. 87-117.

Goto Y (1971) Crack formed in concrete around deformed tension bars. ACI Journal 68(4): 244-251.

Hendriks MAN, de Boer A and Belletti B (2017) Guidelines for Nonlinear Finite Element Analysis of Concrete Structures. Rijkswaterstaat Centre for Infrastructure, Report RTD:1016-1:2017.

Hordijk DA (1991) Local Approach to Fatigue of Concrete. PhD thesis, Delft University of Technology, Delft, The Netherlands.

Husain SI and Ferguson PM (1968) Flexural crack width at the bars in reinforced concrete beams. Research Report Number 102-1F, Center for Highway Research, The University of Texas at Austin, USA.

Jiang DH, Shah SP and Andonian AT (1984) Study of the Transfer of Tensile Forces by Bond. ACI Journal 81(4): 251-259.

Lutz LA (1970) Analysis of Stresses in Concrete Near a Reinforcing Bar Due to Bond and Transverse Cracking. ACI Journal 67(10): 778-787.

Mirza SM and Houde J (1979) Study of Bond Stress-Slip Relationships in Reinforced Concrete. ACI Journal 76(1): 19-46.

Nilson AH (1972) Internal Measurement of Bond Slip. ACI Journal 69(7): 439-441.

Russo G and Romano F (1992) Cracking Response of RC Members Subjected to Uniaxial Tension. Journal of Structural Engineering 118(5): 1172-1190.

Saliger R (1936) High-grade steel in reinforced concrete. Proceedings Second Concress of the International Association for Bridge and Structural Engineering. Berlin-Munich, Germany.

Somayaji S and Shah SP (1981) Bond Stress Versus Slip Relationship and Cracking Response of Tension Members. ACI Journal 78(3): 217-225.

Tammo K, Lundgren K and Thelandersson S (2009) Nonlinear analysis of crack widths in reinforced concrete. Magazine of Concrete Research 61(1): 23-34.

Tammo K and Thelandersson S (2009) Crack behavior near reinforcing bars in concrete structures. ACI Structural Journal 106(3): 259-267.

Tan R, Eileraas K, Opkvitne O et al. (2018a) Experimental and theoretical investigation of crack width calculation methods for RC ties. Structural Concrete https://doi.org/10.1002/suco.201700237: 1-12.

Tan R, Hendriks MAN, Geiker M et al. (2018b) An analytical calculation model for predicting the cracking behaviour of reinforced concrete ties. Under review.

Watstein D and Mathey RG (1959) Width of Cracks in Concrete at the Surface of Reinforcing Steel Evaluated by Means of Tensile Bond Specimens. ACI Journal 56(7): 47-56.

Yannopoulos PJ (1989) Variation of concrete crack widths through the concrete cover to reinforcement. Magazine of Concrete Research 41(147): 63-68.

Accepted manuscript doi:
10.1680/jmacr.18.00156

Table 1. Material parameters of the RC ties investigated in the experiments of Bresler and Bertero (1968) and Yannopoulos (1989).

Material parameters	Bresler and Bertero (1968)		Yannopoulos (1989)	
	Concrete	Steel	Concrete	Steel
Compressive strength, f_c [MPa]	40.8	-	43.4	-
Tensile strength, f_{ct} [MPa]	4.48	-	3.30	-
Yield strength, f_y [MPa]	-	413	-	424
Modulus of elasticity, E_c and E_s [MPa]	33165	205464	32000	200000
Poisson's ratio, ν_c and ν_s	0.15	0.30	0.15	0.30
Tensile fracture energy, $G_f = \frac{73 f_c^{0.18}}{1000}$ [N/mm]	0.142	-	0.144	-
Compressive fracture energy, $G_c = 250 G_f$ [N/mm]	35.6	-	36.0	-

Table 2. CLLM behaviour of $\phi 20c40$ vs. $\phi 32c40$ and $\phi 20c90$ vs. $\phi 32c90$ showing the steel stress σ_s and the corresponding load level F just before a primary crack forms at a distance s_r from the loaded end, mean bond stress $\tau_{bm,x_{cr}}$ of the bond stress distribution over the crack distance x_{cr}, concrete force resultant at the section where a primary crack forms $F_c(x_{cr}) = \tau_{bm,x_{cr}} \pi \phi x_{cr}$ and the cracking force $F_{cr} = f_{ct} A_c$.

RC tie	σ_s [MPa]	F [kN]	x_{cr} [mm]	$\tau_{bm,x_{cr}}$ [MPa]	$F_c(x_{cr})$ [kN]	F_{cr} [kN]
$\phi 20c40$	100.3	31.5	105	3.76	24.8	24.2
$\phi 32c40$	58.1	46.7	109	2.74	30.0	29.0
$\phi 20c90$	341.1	107.1	260	6.23	101.8	99.8
$\phi 32c90$	160.6	129.1	272	4.21	115.1	110.7

Accepted manuscript doi:
10.1680/jmacr.18.00156

Figure 1

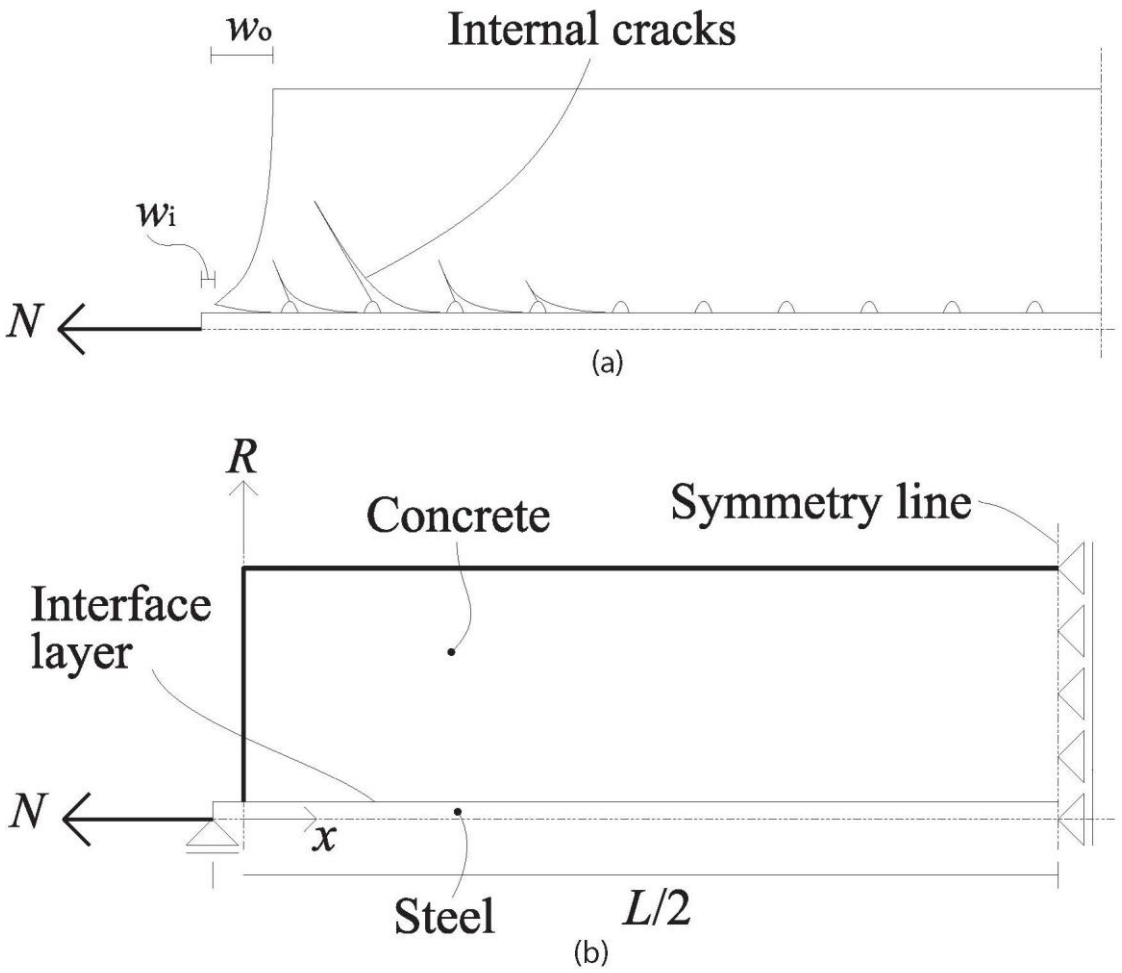

Accepted manuscript doi:
10.1680/jmacr.18.00156

Figure 2

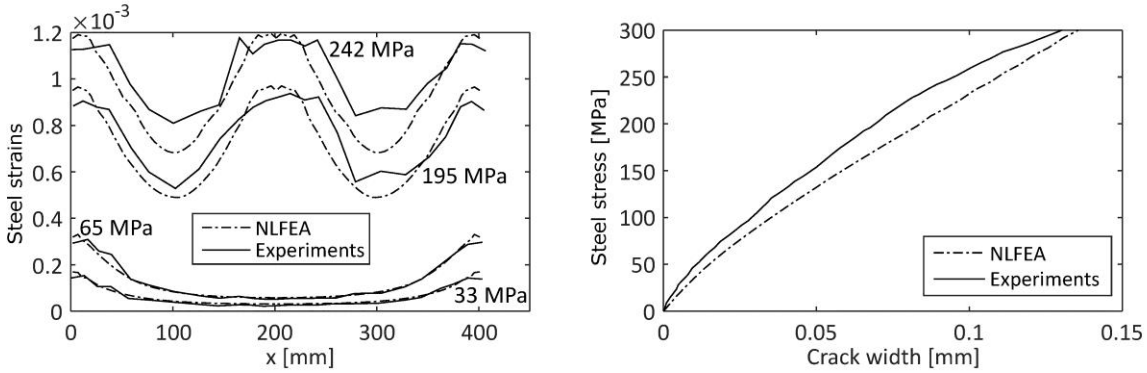

(a) (b)

Accepted manuscript doi:
10.1680/jmacr.18.00156

Figure 3

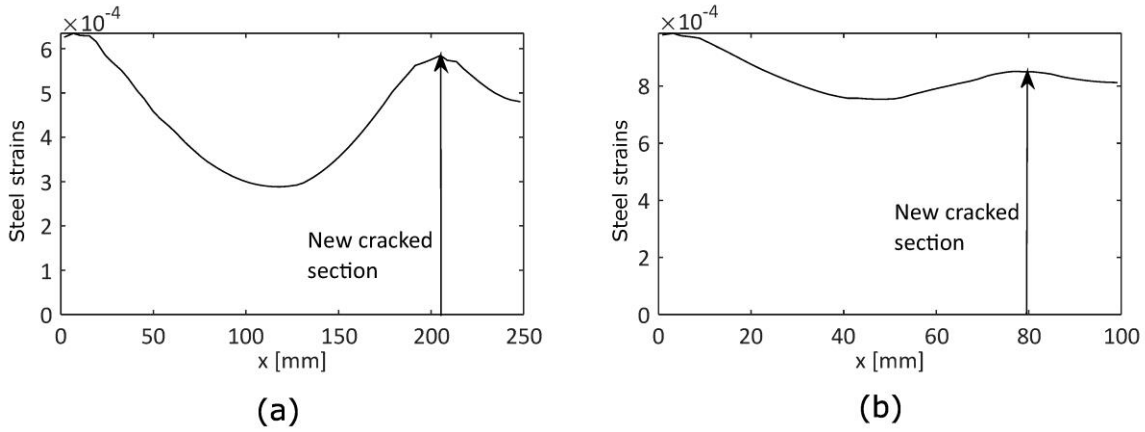

Accepted manuscript doi:
10.1680/jmacr.18.00156

Figure 4

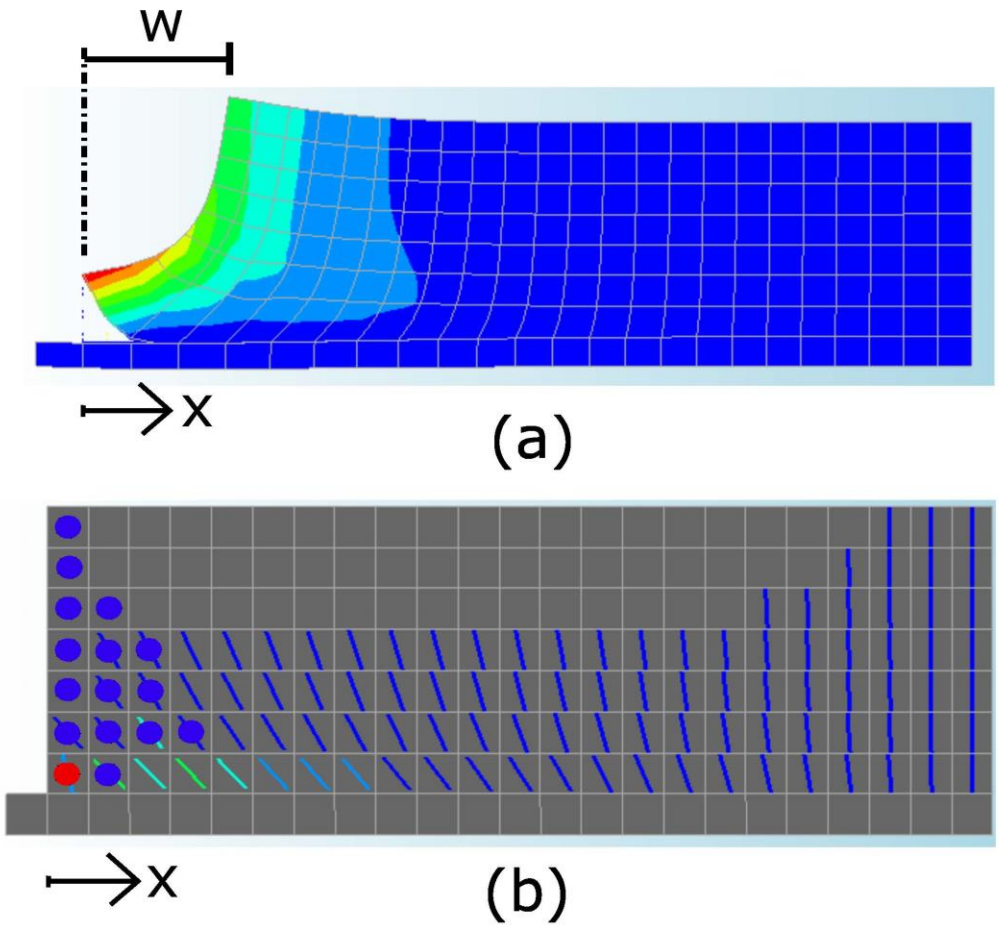

Accepted manuscript doi:
10.1680/jmacr.18.00156

Accepted manuscript doi:
10.1680/jmacr.18.00156

Figure 5

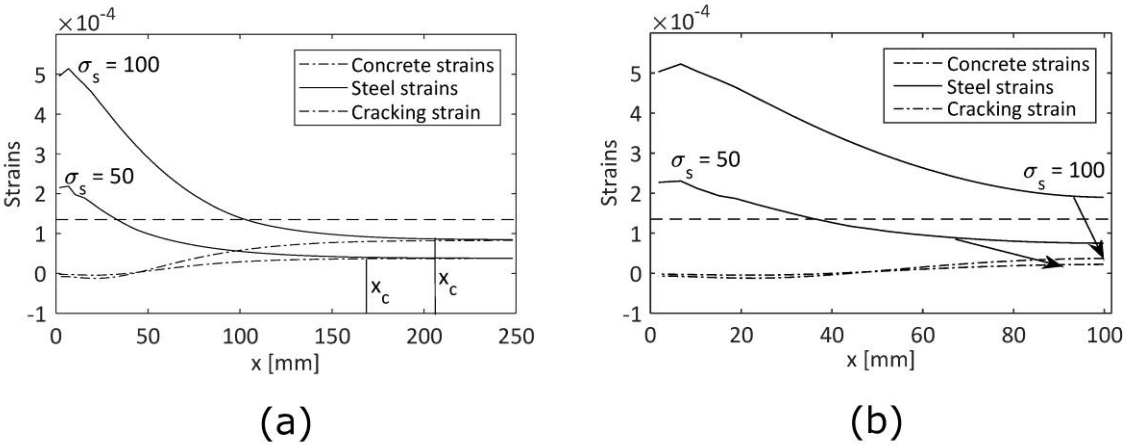

Accepted manuscript doi:
10.1680/jmacr.18.00156

Figure 6

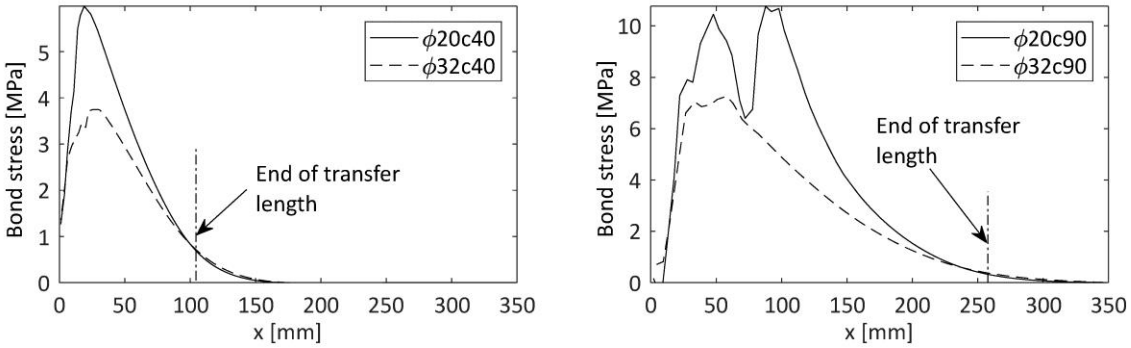

Accepted manuscript doi:
10.1680/jmacr.18.00156

Figure 7

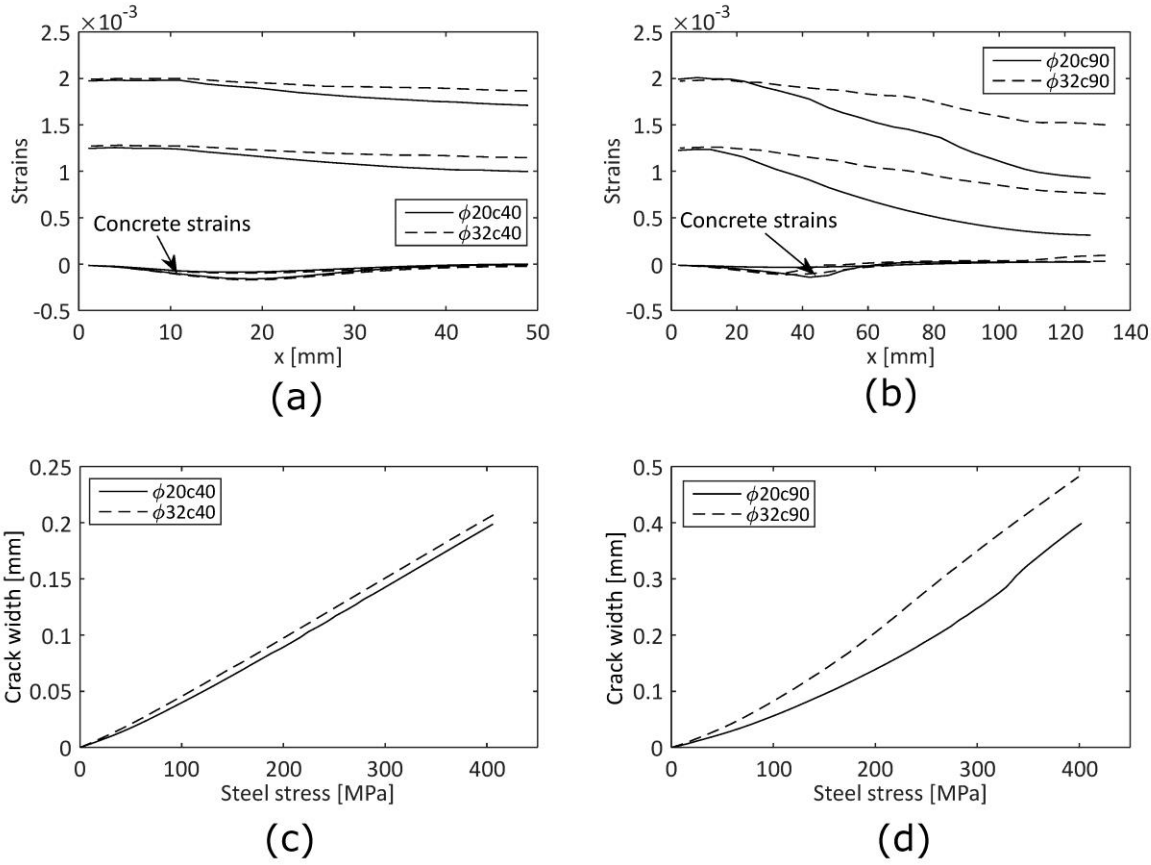

Accepted manuscript doi:
10.1680/jmacr.18.00156

Figure 8

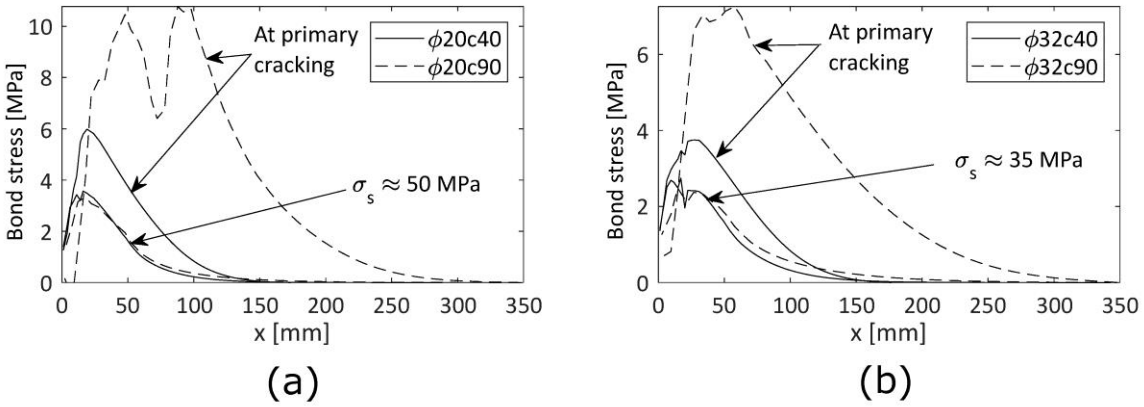

Accepted manuscript doi:
10.1680/jmacr.18.00156

Figure 9

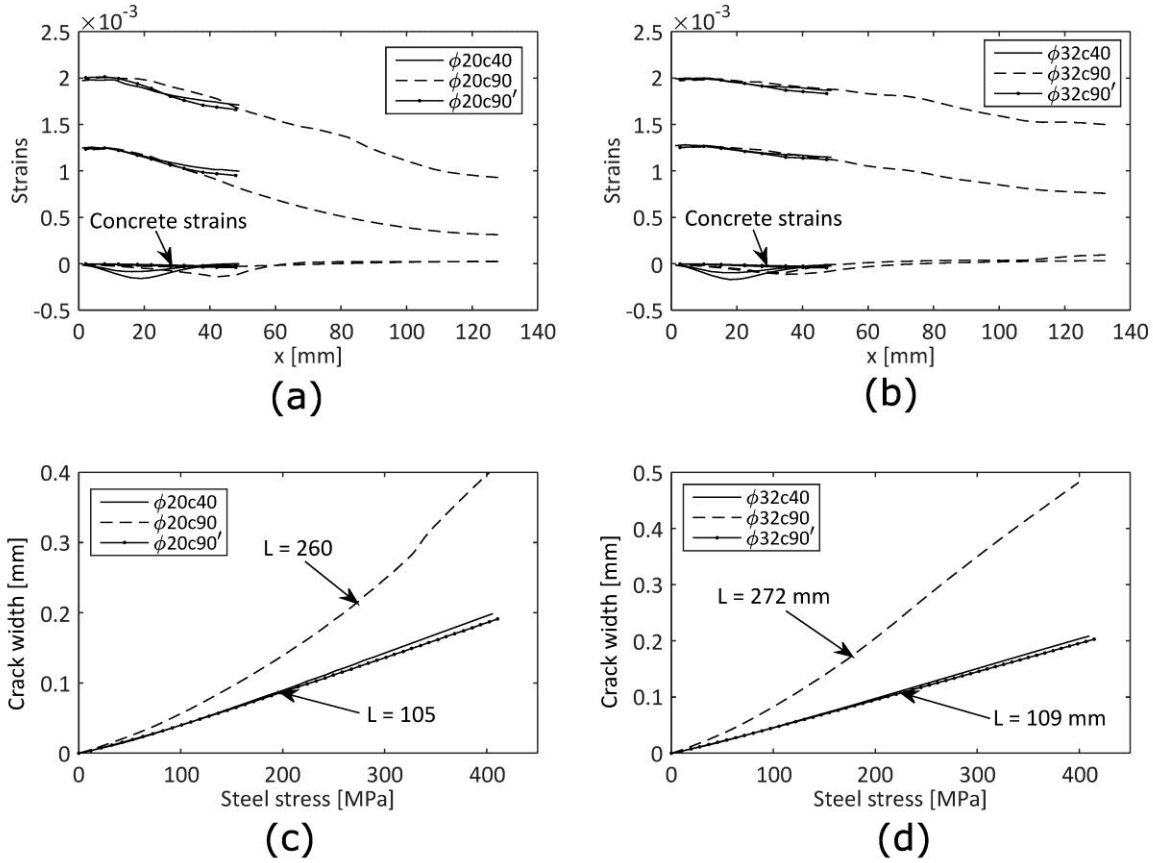

Accepted manuscript doi:
10.1680/jmacr.18.00156

Figure 10

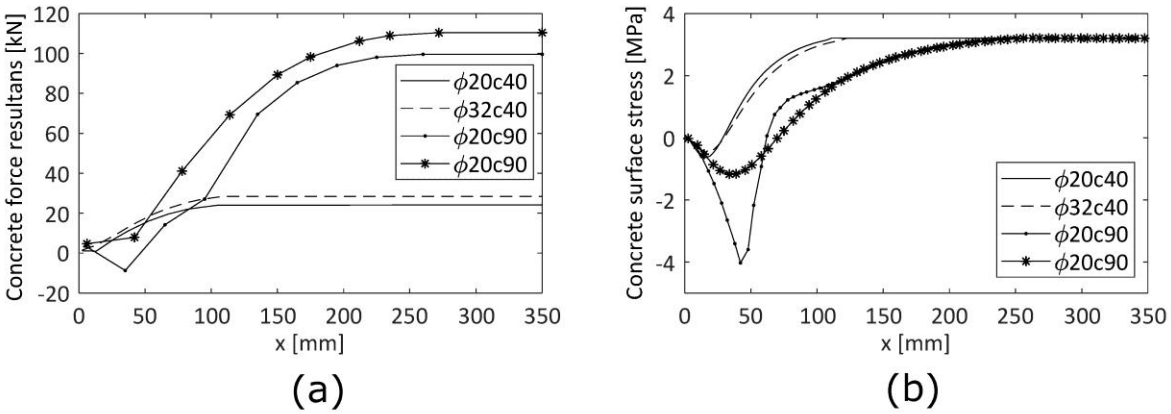

Accepted manuscript doi:
10.1680/jmacr.18.00156

Figure 11

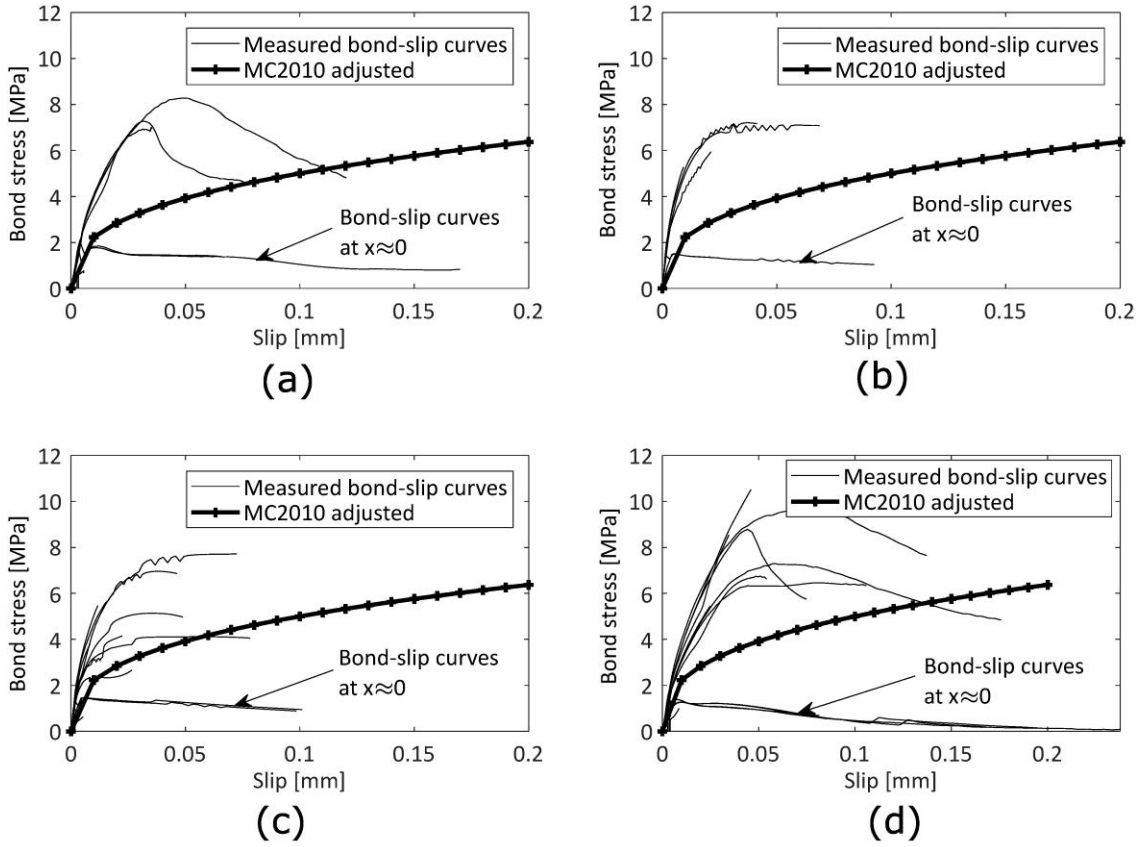

Accepted manuscript doi:
10.1680/jmacr.18.00156

Figure 12

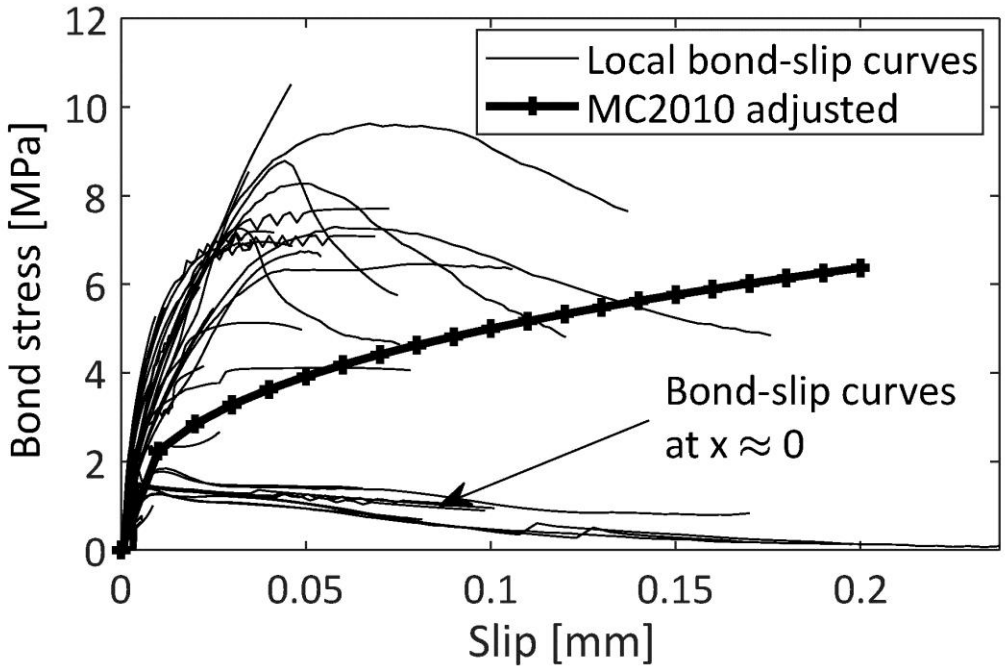

List of figures

Figure 1(a) Typical deformation configuration of RC ties with deformed steel bars. (b) FE-model.

Figure 2(a) Comparison of steel strains in the experiments of Bresler and Bertero (1968) with steel strains obtained in the NLFEA. (b) Comparison of crack widths in the experiments of Yannopoulos (1989) with crack widths obtained in the NLFEA.

Figure 3. Steel strain distributions obtained from the NLFEA immediately after the formation of a new primary crack for the long (a) “Bresler and Bertero” specimen (L = 500 mm) and (b) the long “Yannopoulos” specimen (L = 200 mm).

Figure 4(a) Contour plot of radial displacements and the deformation configuration at $\sigma_s = 180\ \mathrm{MPa}$. (b) Corresponding plot of internally inclined cracks (straight lines) and splitting cracks (circles). (c) Corresponding shear and radial stresses.

Figure 5. Strain distribution for the “Bresler and Bertero” specimen at two similar load levels. (a) CLLM behaviour of a long specimen $L = 500\ mm$. (b) CHLM behaviour of a short specimen $L = 200\ mm$.

Figure 6(a) Bond stress distribution for the CLLM behaviour of $\phi 20c40$ vs. $\phi 32c40$ at primary cracking in accordance with the load levels in Table 2. (b) Bond stress distribution for the CLLM behaviour of $\phi 20c90$ vs. $\phi 32c90$ at primary cracking in accordance with the load levels in Table 2.

Figure 7(a) and (b) Strain distributions respectively for $\phi 20c40$ vs. $\phi 32c40$ and $\phi 20c90$ vs. $\phi 32c90$ at steel stresses $\sigma_s = 250\ \mathrm{MPa}$ and $\sigma_s = 400\ \mathrm{MPa}$. (c) and (d) Development of crack widths with steel stresses respectively for $\phi 20c40$ vs. $\phi 32c40$ and $\phi 20c90$ vs. $\phi 32c90$.

Figure 8(a) Bond stress distribution for the CLLM behaviour of $\phi 20c40$ vs. $\phi 20c90$ at $\sigma_s \approx 50\ \mathrm{MPa}$ and at primary cracking in accordance with the load levels in Table 2. (b) Bond stress distribution for the CLLM behaviour of $\phi 32c40$ vs. $\phi 32c90$ at $\sigma_s \approx 35\ \mathrm{MPa}$ and at primary cracking in accordance with the load levels in Table 2.

Figure 9(a) and (b) Strain distributions respectively for $\phi 20c40$ vs. $\phi 20c90$ and $\phi 32c40$ vs. $\phi 32c90$. (c) and (d) Development of crack widths with steel stresses respectively for $\phi 20c40$ vs. $\phi 20c90$ and $\phi 32c40$ vs. $\phi 32c90$.

Figure 10(a) Development of concrete force resultants over the bar length at cracking. (b) Development of concrete surface stresses over the bar length at cracking.

Figure 11(a) Local bond-slip curves for the “Bresler and Bertero” specimens. (b) Local bond-slip curves for the “Yannopoulos” specimens. (c) Local bond-slip curves for $\phi 20 c 40$ and $\phi 32 c 40$. (d) Local bond-slip curves for $\phi 20 c 90$ and $\phi 32 c 90$.

Figure 12(a) Local bond-slip curves for all of the analysed specimens.

List of notations

A_c	Area concrete
A_s	Area steel
c	Cover
E_c	Modulus of elasticity concrete
E_s	Modulus of elasticity steel
F_c	Force resultant concrete
F_{cr}	Cracking force concrete
f_c	Compressive strength concrete
f_{ct}	Tensile strength concrete
f_y	Yield strength steel
G_f	Tensile fracture energy concrete
G_{fc}	Compressive fracture energy concrete
L	Bar length
N	Applied force at steel bar ends
R	Radial axis
s	Slip
s_1	Slip parameter in bond-slip curve according to MC2010
s_r	Specific distance from the loaded end
t_i	Thickness of interface layer between concrete and steel
w_i	Crack width at the steel bar surface
w_o	Crack width at the specimen surface
x	Position over the bar length
x_{cr}	Crack spacing
x_i	x-coordinate of integration points adjacent to the steel and outer concrete surface
x_r	Transfer length
α	Curve parameter in bond-slip curve according to MC2010
Δx	Half FE length
ε_c	Strains at outer concrete surface
ε_{ci}	Concrete strains at integration points
ε_{ct}	Cracking strain concrete
ε_s	Strains at steel surface
ε_{si}	Steel strains at integration points
ν_c	Poisson's ratio concrete
ν_s	Poisson's ratio steel
ρ_{eff}	Reinforcement ratio
σ_s	Steel stress

τ_1	Bond stress parameter in bond-slip curve according to MC2010
$\tau_{\mathrm{bm},x_{\mathrm{cr}}}$	Mean bond stress over the crack distance
ϕ	Bar diameter